KSCE Journal of Civil Engineering (2011) 15(8):1381-1394
DOI 10.1007/s12205-011-1225-6

Structural Engineering
www.springer.com/12205

Damage Evaluation of Composite-special Moment Frames with Concrete-filled Tube Columns under Strong Seismic Loads

Taehyo Park*, Won-Sup Hwang, Roberto T. Leon***, and Jong Wan Hu******

Received May 27, 2010/Accepted February 9, 2011

Abstract

Concrete Filled steel Tube (CFT) columns have been widely used in moment resisting frame structures located on non-seismic zones or high seismic zones. This paper discusses the design of such composite members based on the advanced methods which are introduced in the 2005 America Institute of Steel Construction (AISC) Specification and the 2005 AISC Seismic Provisions. These design specifications explicitly allow the use of the full plastic capacities of CFT columns, and so they require column members with more slender steel walls than ones allowed in previous specification. In addition, this study focuses particularly on damage evaluation following nonlinear frame analyses. The paper begins with an examination of design interaction curves including the length effect and the full plastic strength demand in CFT beam-column members. Based on advanced computational simulations of a series of 3-, 9-, and 20-story SAC composite-special moment frames, this paper then investigates new techniques to evaluate the damage of CFT columns during a strong earthquake. The paper concludes with some discussion of (a) step by step procedures to compute the interactive ratios of the individual CFT beam-columns and (b) member vs. seismic performance evaluation.

Keywords: *concrete-filled tube columns, composite-special moment frame, nonlinear frame analyses, interaction curves, damage evaluation, plastic strength ratios*

1. Introduction

Moment-resisting frames have traditionally used for the lateral-force resisting system in the area of the high seismicity because they have significant potential for large ductility under seismic loading. They also provide the limited interference with other building systems (Grecea *et al*., 2004; Asgarian *et al*., 2010). Recently, these moment-resisting frames have been suggested in composite construction. During the late 1980s, the design profession began to exploit the synergistic action of combining concrete and steel in the seismic design using the practice which focuses on steel beams with composite steel and concrete columns (Wu *et al*., 2005). Constructional advantages for the synergistic effect between two materials are based on the fact that concrete products relatively low material costs, good fire resistance, and easy fabrication, while steel provides high toughness, ductility, and relatively high strength-to-weight ratios (Wu *et al*., 2007; Tsai *et al*., 2008; Kim *et al*., 2008; Chin *et al*., 2009; Hu and Leon, 2010). These advantages have stimulated the development of composite-moment frame systems extensively used in Japan. The composite-moment frame systems have incorporated with special moment frames which must satisfy the detailing requirements of moment connections to provide a substantial amount of toughness and ductility, implying excellent inelastic energy dissipation and acceptable seismic performance. Composite-Special Moment Frames (C-SMFs), which rely on the flexibility of steel beam-to-composite column connections for inelastic response, were developed with this motivation. The development of C-SMFs has increasingly taken place in practice, and there have been recent researches resulting in practical design recommendations (Azizinamini and Schneider, 2004; Ricles *et al*., 2004; Hu *et al*., 2011).

There are two kinds of composite columns which are (1) Steel-Reinforced Concrete section (SRC) columns and (2) Concrete Filled Tube (CFT) columns. The use of these composite columns in the USA has been limited to perimeter-moment frame structures in high-rise buildings which are susceptible to strong seismic or wind forces (Roeder, 1998; Calambos, 2000). In the case, the steel section has been often used for the election purposes so as to carry the gravity loads, later with a large confined concrete section provided for the stiffness to resist the lateral forces in tall buildings. Generally, more additional advantages

*Member, Professor, Dept. of Civil and Environmental Engineering, Hanyang University, Seoul 133-791, Korea (E-mail: cepark@hanyang.ac.kr)
**Member, Professor, Dept. of Civil Engineering, Inha University, Incheon 402-751, Korea (E-mail: hws@inha.ac.kr)
***Professor, School of Civil and Environmental Engineering, Georgia Institute of Technology, Atlanta, GA, 30332, USA (E-mail: rl58@ce.gatech.edu)
****Associate Research Fellow, R&D Strategy & Investment Analysis Division, Office of National R&D Investment Strategy and Analysis, Korea Institute of S&T Evaluation and Planning (KISTEP), Seoul 137-130, Korea (Corresponding Author, E-mail: jongp24@kistep.re.kr)

can be observed at the CFT construction in comparison with the SRC construction because: (a) the steel section increases the strength and ductility of concrete owing to its confining effect, (b) concrete prevents local buckling, and (c) steel tubes are also accepted as the mold for casting concrete in construction. Thus, CFT columns are accepted for the design of C-SMF structures proposed in this study.

The current AISC design code provisions for composite construction - namely, the 2005 AISC Specification and Seismic Provisions for structural steel buildings (ANSI/AISC 360-05, 2005; ANSI/AISC 341-05, 2005) - are increasingly presenting engineers with the new guidance on the analysis and design of composite columns and composite-moment frames. This paper provides a detailed background to their development. It offers design examples and discussions to supplement SAC post-Northridge frame models as reference examples which are included in the FEMA 355C (2000). For the analytical study of composite frame models, they were modeled as numerical frame ones including both two dimensional (2D) joint models for connections and discrete fiber sections for composite columns.

Accordingly, the purpose of this research is to examine the behavior of CFT beam-columns and to estimate maximum strength for composite cross sections. Consequently, it can be shown that plastic capacities for rectangular/circular CFT beam-columns are estimated with quite reasonable accuracy using the axial force and moment (P-M) interaction formulas for composite columns. Finally, based on the analytical study of CFT beam-column sections, new advanced analysis guidelines from computational investigation and damage evaluation conducted on 3-, 9-, and 20-story C-SMFs are presented in this research.

2. Overall Research Scope

The case studies are composed of composite CFT cross section analyses and 2D nonlinear frame analyses. The numerical experiments were performed by using a nonlinear structural analysis program, OpenSEES v.1.7.3 (Mazzoni *et al*., 2006).

The structural shapes of composite beam-columns become circular or rectangular concrete-filled steel tubes (CCFT or RCFT). The test specimens for composite cross sections were subjected to a constant axial load plus increasing bending moments. Fiber models consisting of steel fibers and concrete fibers were developed for high strength CFT beam-columns by using 2D fiber sections which are available in the OpenSEES program. The moment-curvature response ($M-\phi$) of CFT specimens was measured in order to estimate the overall capacity of composite CFT beam-columns. P-M interaction curves were formulated for composite CFT beam-column specimens by using the fiber analyses. The accuracy of P-M interaction formulas can be verified through comparison with the result of fiber analyses.

The SAC post-Northridge frame models provided by the FEMA 355C were used for the design of 3-, 9-, and 20-story C-SMFs with CFT columns. For nonlinear frame analyses, these frames were modeled as numerical 2D frame models. One of the most significant characteristic of the 2D frame models proposed in this study is the careful consideration of both panel zone modeling for moment connections and 2D discrete fiber sections for composite cross sections. The real behavior of composite connections was replicated using a robust 2D joint element as described in the original investigation (Altoontash, 2004).

Within nonlinear frame analyses, nonlinear dynamic analyses were run for a set of 2% in 50 year ground motions (Somerville *et al*., 1997). Assessment methods implemented in composite CFT beam-columns were extended into these nonlinear frame analyses. To accomplish the damage evaluation, the demand at the composite cross sections must be established from advanced computational simulations which were carried out on a series of entire composite frame models. The structural damage was estimated in this study through comparisons of the plastic strength ratios (PSRs) which are defined as the ratios of the demand to the strength capacity for the member cross section from the P-M interaction formulas. Besides investigation of the statistical values of PSRs distributed over the lower story levels, the sequence of stress hinges was also examined in this study.

3. Design Equations for P-M Interaction Diagrams

The 2005 AISC Specification includes the design guideline for composite columns consisting of rolled or built-up structural steel shapes, pipe or Hollow Steel Section (HSS), and structural concrete component acting together as a composite member. Especially, this specification distinctly accepts the theory of the full plastic stress distribution based on the assumption of linear strain across the section height and perfectly elasto-plastic material behavior. With this simple assumption, the nominal strength shall be estimated by assuming that steel has reached yield stress under either tension or compression and that concrete has reached crushing strength under only compression as shown in Tables 1 and 2. The geometry notations for calculation are also given to both tables. Corresponding stress on a rectangular concrete stress block and on a circular concrete stress block is typically taken as $0.85f_{cc}$ and $0.95f_{cc}$, respectively. The P-M interaction diagrams for a composite section can be generated as a linear interpolation between five points. The generation of these points on the P-M interaction diagram involves the selection of a plastic neutral axis (PNA) location as shown in both tables. In other word, the P-M interaction can be generated by moving the location of the PNA according to a different combination of axial force and bending moment.

For five component points, Point (A) and Point (B) indicate to the pure axial strength and the pure flexural strength of the section, respectively. Point (C) is anchored to the relatively same PNA position from the center axis corresponding to that of Point (B), so it contains the same flexural capacity as Point (B) and the same magnitude as the axial resistance from the pure concrete part. In Point (D), the PNA position is identical to the center axis. As a result, the maximum flexural strength and one half of axial strength of that determined for Point (C) can be shown. Point (D)

Table 1. Summary of Nominal P-M Interaction Diagram Formula for RCFT Columns

PLASTIC CAPACITIES FOR COMPOSITE FILLED HSS BENT ABOUT ANY AXIS

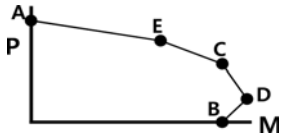

Section	Stress Distribution	Point	Defining Equations
	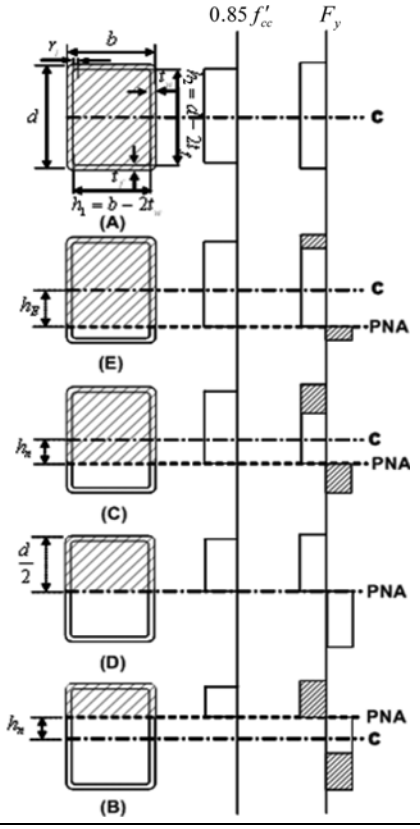	A	$P_A = A_s F_y + 0.85 f'_{cc} A_c \quad M_A = 0$ A_s = *Area of steel shape* $\quad A_c = h_1 h_2 - 0.858 r_i^2$
		E	$P_E = \frac{1}{2}(0.85 f'_{cc} A_c) + 0.85 f'_{cc} h_1 h_E + 4 F_y t_w h_E$ $M_E = M_{\max} - \Delta M_E \quad \Delta M_E = Z_{sE} F_y + \frac{1}{2} Z_{cE}(0.85 f'_{cc})$ $Z_{sE} = b h_E^2 - Z_{cE} \quad Z_{cE} = h_1 h_E^2 \quad h_E = \frac{h_n}{2} + \frac{d}{4}$
		C	$P_C = 0.85 f'_{cc} A_c \quad M_C = M_B$
		D	$P_D = \frac{(0.85 f'_{cc} A_c)}{2} \quad M_D = Z_s F_y + \frac{1}{2} Z_c (0.85 f'_{cc})$ $Z_s = \frac{b d^2}{4} \quad Z_c = \frac{h_1 h_2^2}{4} - 0.192 r_i^3$
		B	$P_B = 0 \quad M_B = M_D - Z_{sn} F_y - \frac{1}{2} Z_{cn}(0.85 f'_{cc})$ $Z_{sB} = 2 t_w h_n^2 \quad Z_{cB} = h_1 h_n^2$ $h_n = \frac{(0.85 f'_{cc} A_c)}{2(0.85 f'_{cc} h_1 + 4 t_w F_y)} \le \frac{h_2}{2}$

results in the balance point. Point (E) is an additionally arbitrary point to better describe the effect of flexural strength in an interaction diagram. The following equations summarized in Tables 1 and 2 are reasonably accurate and conservative to estimate the cross-sectional strength.

After the cross-sectional strength has been determined, the P-M interaction diagrams need to be reduced to include the stability effect. The compressive strength for only axially-loaded CFT columns (P_{cr}) should be determined in accordance with the column slenderness (a). The following calculations to determine the compressive strength are given to Table 3 (ANSI/AISC 360-05, 2005). To take the stability effect into consideration, the values of axial loads (P) should be reduced in proportion to the compressive strength ratio of P_{cr} to P_A. Once the initial column members are selected, the cases for P-M interaction surfaces according to the composite cross section will be presented.

4. Frame Design

C-SMFs were designed on the basis of reference examples provided by the SAC model structures (FEMA-355C, 2000). They have been used to evaluate the performance of new or updated structural systems in the aftermath of 1994 Northridge and 1995 Kobe earthquakes. In this study, six ordinary office buildings were designed with 3-, 9-, and 20-story SAC post-Northridge composite-moment frames. They were assumed to be located on a stiff soil area of Los Angeles area. The plan and elevation views of SAC model buildings are shown in Fig. 1. The members selected for the steel beams are also shown in this figure. Moment connections were marked by the thick lines located along the perimeter frames. Only perimeter moment frames were designed to resist seismic lateral loads. On the other hand, the interior gravity frames marked by thin dash lines were connected by simple pin connections. The CFT column bases were assumed to be fixed in the 3-story building, while the CFT column bases in the 9- and 20-story building were modeled as pinned-end supports. The 9-story buildings have a single-level basement, and the 20-story buildings have a 2-level basement. Their basement levels were restrained against lateral movement. It should be noted that the post-Northridge design for 3-, 9-, and 20-story buildings requires moment bays in each direction to satisfy the redundancy, which is related to the end support con-

Table 2. Summary of Nominal P-M Interaction Diagram Formula for CCFT Columns

PLASTIC CAPACITIES FOR COMPOSITE FILLED ROUND HSS BENT ABOUT ANY AXIS

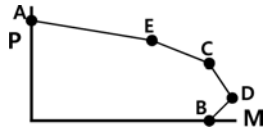

Section	Stress Distribution	Point	Defining Equations
	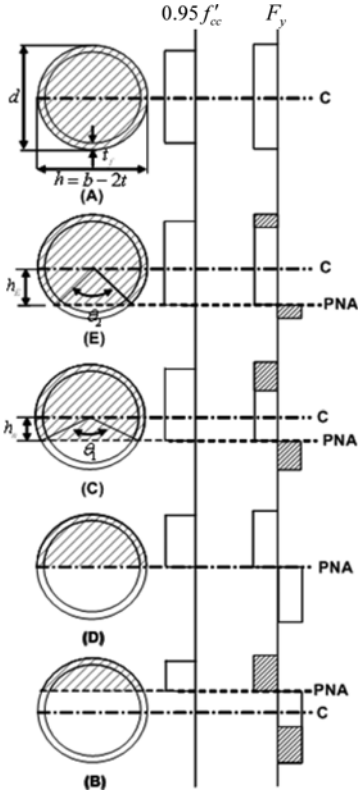	A	$P_A = A_s F_y + 0.95 f'_{cc} A_c \quad M_A = 0$ $A_c = \frac{\pi h^2}{4} \quad A_s = 2\pi r_m t \quad r_m = \frac{d-t}{2}$
		E	$P_E = (0.95 f'_{cc} A_c + F_y A_s) - \frac{1}{2}\left[F_y(d^2-h^2) + \frac{1}{2}(0.95 f'_{cc})h^2\right]\left[\frac{\theta_2}{2} - \frac{\sin\theta_2}{2}\right]$ $M_E = Z_{sE} F_y + \frac{1}{2} Z_{cE}(0.95 f'_{cc})$ $h_E = \frac{h_n}{2} + \frac{d}{4} \quad Z_{sE} = \frac{d^3 \sin^3(\theta_2/2)}{6} - Z_{cE} \quad Z_{cE} = \frac{h^3 \sin^3(\theta_2/2)}{6}$
		C	$P_C = 0.85 f'_{cc} A_c \quad M_C = M_B$
		D	$P_D = \frac{0.95 f'_{cc} A_c}{2} \quad M_D = Z_s F_y + \frac{1}{2} Z_c (0.95 f'_{cc})$ $Z_s = \frac{d^3}{6} - Z_c \quad Z_c = \frac{h^3}{6}$
		B	$P_B = 0 \quad M_B = Z_{sB} F_y + \frac{1}{2} Z_{cB}(0.95 f'_{cc})$ $Z_{sB} = \frac{d^3 \sin(\theta_1/2)}{6} - Z_{cB} \quad Z_{cB} = \frac{h^3 \sin(\theta_1/2)}{6}$ $\theta_1 = \frac{0.026K_c - 2K_s}{0.0848K_c} + \frac{\sqrt{(0.026K_c + 2K_s)^2 + 0.857K_c K_s}}{0.0848K_c}$ $K_c = f'_c h^2 \quad K_s = F_y r_m t \quad h_n = \frac{h}{2}\sin\left(\frac{\pi - \theta}{2}\right) \le \frac{h}{2}$

Table 3. Computation of Compressive Strength Capacity for Composite Columns

COMPRESSIVE STRENGTH CAPACITY FOR COMPOSITE COLUMNS

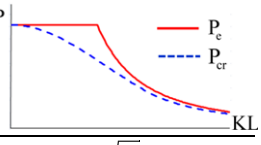

Slenderness Limit	$d/t < 0.15\left(\frac{E_s}{F_y}\right)$ for CCFT $\quad b/t < 2.26\left(\sqrt{\frac{E_s}{F_y}}\right)$ for RCFT
Defining Equations	$C_3 = 0.6 + \left(\frac{A_s}{A_c + A_s}\right) \le 0.9 \quad EI_{eff} = E_s I_s + C_3 E_c I_c$ $I_s = \frac{\pi}{64}[d^4 - (d-2t)^4] \quad I_c = \frac{\pi(d-2t)^4}{64}$ $P_e = \frac{\pi^2 EI_{eff}}{(KL)^2} \quad P_o = A_s F_y + C_1 f'_{cc} A_c$ $C_1 = 0.85$ for RCFT $\quad C_1 = 0.95$ for CCFT $\alpha = \sqrt{\frac{P_o}{P_e}}$ $P_{cr} = P_o(0.658^{\alpha^2}) \quad (\alpha \le 1.5)$ $P_{cr} = 0.877 P_e \quad (\alpha > 1.5)$

dition, as defined in the FEMA 355C.

This soil condition for LA buildings was soil type D in the ASCE 7-05 (2005). The response spectra corresponding to an ensemble of 2% in 50 year ground motion and a return period of 2475 years were applied to the building design. The buildings in LA area were designed by using the mapped spectrum accelerations (LA 90045 area) corresponding to S_S = 1.60 g for the short period and S_1 = 0.60 g for 1 second period. The mass conformed to the code requirement for seismic design as specified in Appendix B of the FEMA 355C. It included gravity loads plus partial live loads. The importance factor (I_E) of 1.0 was assigned to the buildings in accordance with Occupancy Category I or II. Special composite steel and concrete moment frame systems, as specified in Table 12.2-1 of the ASCE 7-05, were selected to determine the response modification factor (R) and the deflection amplification factor (C_d) for C-SMF structures. Other basic conditions applied to the building design are summarized in Table 4.

The SAC post-Northridge composite-moment frames were constructed using seven different sections of either RCFT columns or CCFT columns to take different frame configurations into consideration. The interior columns required larger member sizes than the exterior ones to withstand more gravity loads. The initial

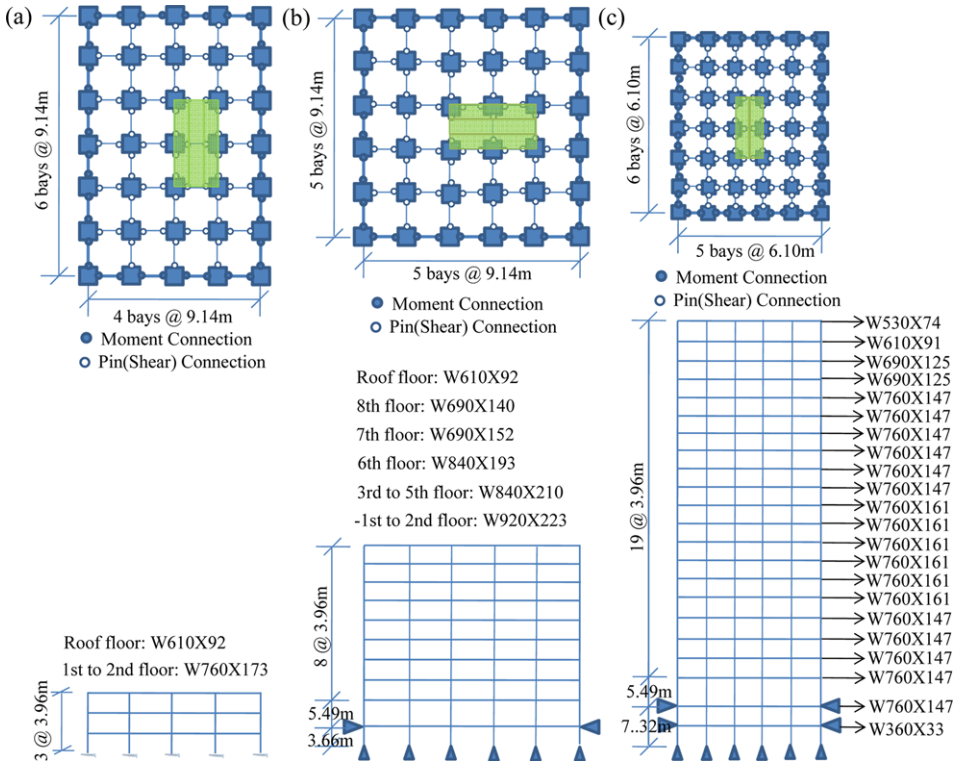

Fig. 1. Floor Plans and Elevations for Composite-moment Frames: (a) 3 Story Bay, (b) 9 Story Bay, (c) 20 Story Bay

Table 4. Basic Conditions Applied to the Composite-moment Frame Design

Located Area	Gravity Loads	SDC	Site Condition	Occupancy Category
LA Area	Dead: 4.12 kPa Live: 2.39 kPa	D Class	Stiff Soil (Site Class D)	Ordinary Structures

Table 5. The Size of CFT Columns (SI unit)

Model ID	RCFT Column		Model ID	CCFT Column	
	Exterior Column	Interior Column		Exterior Column	Interior Column
3SRCFT	HSS254X254X10	HSS254X254X10	3SCCFT	HSS286X12	HSS286X12
9SRCFT	HSS406X406X12	HSS406X406X16	9SCCFT	HSS457X457X12	HSS508X508X12
20SRCFT	HSS356X356X16	HSS406X406X16	20SCCFT	HSS457X457X12	HSS508X508X12

selection of CFT column members is given to Table 5. The first number and letter of the acronym shown in the model ID indicate the total numbers of stories (i.e. 3S or 9S). The remainder of the letter indicates the CFT column type used (i.e. RCFT: Rectangular CFT, CCFT: Circular CFT). A uniform size for all column members over the story height was selected on either exterior or interior columns because of fabrication and economy consideration.

After the selection of initial member sizes, the design check of deflection and drift limit for proposed moment frames subjected to the dominant load combination (i.e. LC5 specified in the ASCE 7-05) should be conducted for the structural safety. The safe design of composite-moment frame models was achieved in the observation of elastic analysis results. These elastic analyses were used to evaluate inter-story drift, deflection, and P-Delta effects. The safe design check was conducted on an achievement that inter-story drift should be less than or equal to the allowable inter-story drift as obtained from Table 12.12-1 of the ASCE 7-05 for any story levels. The inter-story drift can be calculated as the difference of elastic deflections between top and bottom of each story level. In addition, the stability to consider P-Delta effect should not exceed the stability coefficient limit as also specified in the ASCE 7-05. The more detail examination on the design verification applied to the proposed composite-moment frames was performed on the companion paper (Hu *et al*., 2010).

5. Analytical Models for C-SMF with CFT columns

Because of symmetry and the assumption of rigid floor diaphragms, 2D perimeter frames can be considered as the representative of the typical frame behavior. Thus, perimeter moment frames shown in Fig. 1 were modeled as 2D numerical frame models for nonlinear frame analyses. The modeling attributes for these numerical models are described in Fig. 2. They

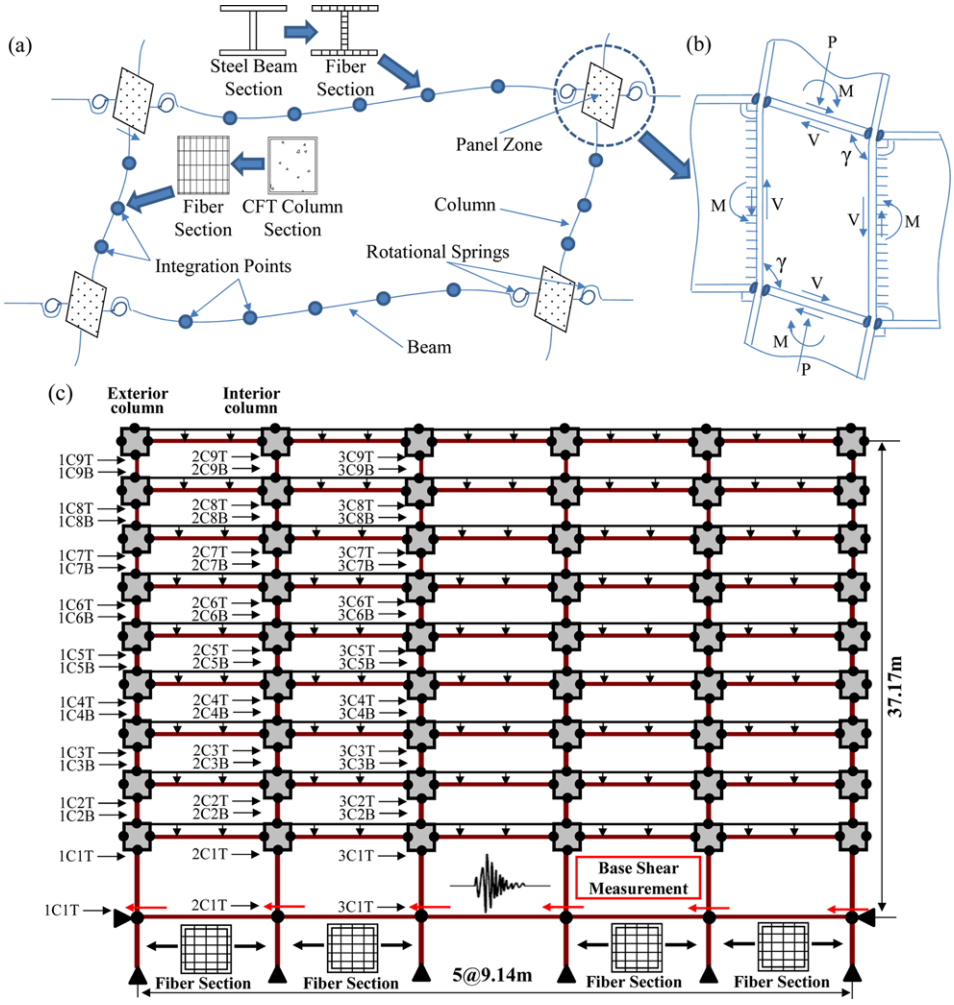

Fig. 2. Numerical Modeling Attributes for Composite-moment Frames (C-MF) Including Panel Zone Model with Rigid Boundary Elements and Nonlinear Beam-column Elements with 2D Fiber Sections: (a) Deformed C-MF Under Seismic Loading; (b) Deformed Panel Zone Subjected to Seismic Loading; (c) Detail Numerical Modeling Attributes for Applied Loads, Response Measurement, Panel Zone, Elevation View, and Column IDs for Observation (9SRCFT)

contained refined panel zone modeling, material nonlinearity, and 2D fiber section. The general modeling methods for numerical frame models are introduced in FEMA 355C. All nonlinear frame analyses were also carried out under the conditions which are provided by this guideline.

The composite CFT columns and steel beams were made up of nonlinear beam-column elements. As shown in Fig. 2(a), the cross sections of CFT columns and steel beams were modeled as 2D discrete fiber sections which are placed in the integration points of nonlinear beam-column elements. The output information including member forces may be extracted at these given points, using the OpenSEES element recorder tool. Fig. 2(c) explains the modeling attributes for the applied loads, ground accelerations, elements, cross sections, panel zones, and response measurements with more details.

The material constitutive models for confined concrete with the geometric property were generated by using the equations proposed by Hu *et al*. (2005). The corresponding nonlinear stress-strain curve including the notations associated with the equations is given to Fig. 3. Owing to the laterally confining pressure (f_l), the maximum uni-axial compressive strength of confined concrete was larger than that of unconfined concrete ($f'_{cc} > f'_c$). The material property of confined concrete was determined by this constitutive model.

The expected material strengths were based on the material properties shown in Fig. 4. The material properties for steel and concrete members were simulated by default nonlinear material models which were provided in the OpenSEES program, and then were assigned into the nonlinear elements with the 2D fiber sections. FE350 (A572-Gr.50) carbon steel was used for the steel tube of RCFT columns, while FE310 (A500-Gr.B) carbon steel was used for that of CCFT columns as specified in the AISC-LRFD code (2001). The material behavior of concrete inside the CFT column contains different stress-strain curves under tension-compression loads and confined effect generated by outside steel tube. The uni-axial compressive strength was much larger than uni-axial tensile strength as shown in Figs. 4(c) and 4(d). Moreover, the gentle strength degradation after peak crushing strength was

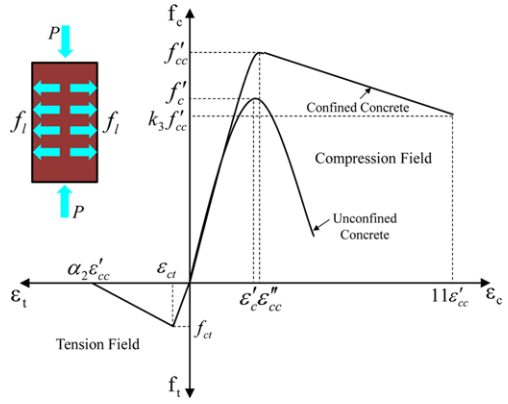

Fig. 3. Stress and Strain Curve for the Concrete Material (Hu *et al*., 2005)

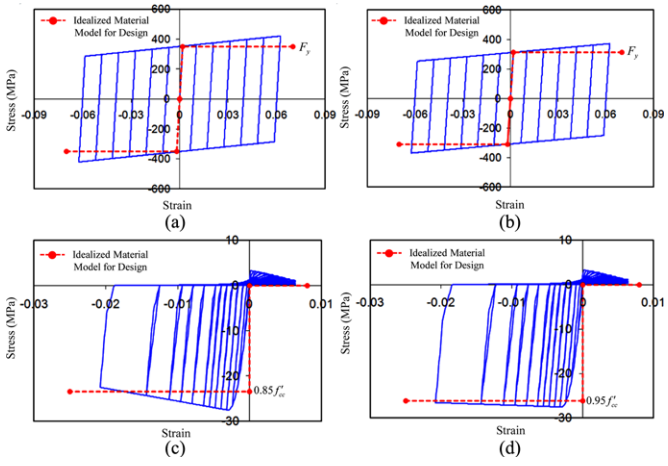

Fig. 4. Material Properties for the Analyses: (a) Stress and Strain Curve for FE350 Steel [A572-Gr.50], (b) Stress and Strain Curve for FE310 Steel [A500-Gr.B], (c) Stress and Strain Curve for Confined Concrete (RCFT), (d) Stress and Strain Curve for Confined Concrete (CCFT)

due to the confined effect. The compressive strength of concrete in the circular section deteriorates more slowly than that in the rectangular section on the ground that the steel tubes with circular sections provide relatively stronger lateral support to inside concrete core under axial compressive force than those with rectangular sections (Hu *et al*., 2005). The bi-linear elasto-plastic curves are also plotted as dashed lines on Figs. 4(a) to 4(d). The plastic strength capacity for composite cross sections (see Tables 1 and 2) was estimated using ideal rigid-plastic models considered as a conservative approximation for the section design.

Besides refined material models, the panel zone modeling reasonably to simulate the behavior of connections was taken into account by using the precise 2D joint element which was originally developed by Altoontash (2004) (see Fig. 5). The steel beam-to-composite column connections in the numerical frame model were made up of these joint elements as shown in Fig. 2(c). The idealized force distribution at the deformed connection subjected to seismic loads is shown in Fig. 2(b). The beam

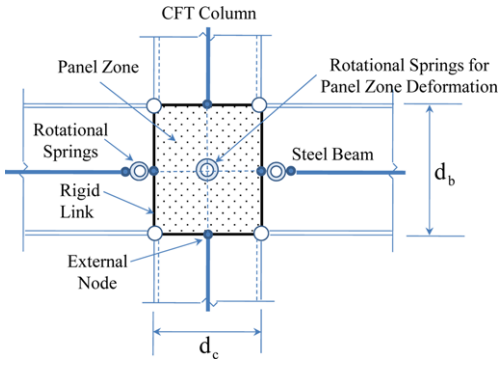

Fig. 5. Numerical Panel Zone Model with Rigid Boundary Elements

carries the flexural bending moment (M) and develops plastic hinge mechanism. On the other hand, the composite column carries the axial gravity load (P). Moreover, the composite panel zone at the connection deforms by the internal shear force forces (V) transformed from bending moments. To simulate the exact behavior of connections under these response mechanisms, the 2D joint element was composed of nodes, zero-length rotational springs, and rigid boundary rinks. As shown in Fig. 5, the finite size of the panel zone was taken into account by the rigid boundary rinks enveloped in 4 external nodes. The nonlinear moment-rotational behavior of connections was simulated by the zero-length rotational springs installed on the external nodes of steel beam ends. The CFT columns were directly connected to the external nodes without any rotational springs in order to carry the gravity axial loads elastically. The shear distortion at the panel zone was simulated by rigid boundary rinks incorporated with the shear panel spring. This spring was installed on the center of the panel zone (see Fig. 5). The tri-linear behavior of the composite panel zone including yield and ultimate shear strength was simulated using analytical predictions proposed by Nishiyama *et al*. (2004), and then was assigned into the shear panel spring.

Moment connections utilized in the moment resisting frame system have been designed with the design strength which depends on the full plastic capacity of the steel beam under flexural moment load. It means that the plastic hinge, as the first failure mode, generally occurs at the beam. In addition, the rotational angle limit for the connection design should be required to obtain the ductile behavior over the certain range of the total rotational angle demand (Leon, 1997). For instance, the total rotational angle of 0.04 radians consisting of an elastic rotation of 0.01 radians and a plastic rotation of 0.03 radians under reversed cyclic loading has been accepted as the requirement for the ductile system in the aftermath of 1994 Northridge earthquake (Leon, 1997). Therefore, the ductile connections are characterized by no flexural strength degradation up to the total rotational angle of 0.04 radians.

The steel beam-to-CFT column connection with a diaphragm continuous through the steel tube was accepted for the connection system used in the proposed moment frames. The cyclic

behavior of this connection type obtained from the experimental test results is shown in Fig. 6. The physical experiments were performed by Schneider and Alostaz (1998). There was no flexural strength degradation until the total rotational angle of 0.06 radians. The flexural strength began to deteriorate slowly when the local buckling of the beam flange occurred. The ultimate moment was approximately 1.25 times the full plastic moment of the steel beam. As a result, the connection design satisfies the requirement of the connection used in the C-SMF with respect to the limit of strength and rotation. As shown in Fig. 6, the moment-rotation angle curve simulated by the 2D joint element is compared with that obtained from the experimental test in order to validate the adequacy of the numerical joint modeling. The simulated curve was calibrated to the experimental cyclic response, so the simulated curve shows good agreements with the experimental test result in terms of the significant attributes such as initial slope, ultimate strength, strength degradation, and Bauschinger effect.

For the analytical study, nonlinear frame analyses accepted the Newton-Raphson iteration algorithm to ensure static equilibrium at each time step. They were performed by implicit integration using the Newmark-Beta constant acceleration method. The structural damping ratio defined by the Rayleigh command in the OpenSEES program was assumed to be 0.025. The equivalent point masses were assigned to all joints so as to generate the story shear forces due to the ground acceleration. Two suites of ground motions with 2% probability of exceedence in 50 years for the western US area (Los Angeles (LA) and Seattle (SE) area) were used for nonlinear dynamic analyses. They consist of 40 ground motions (LA21 to LA40 and SE21 to SE40) developed from both historical records and simulations as a part of the FEMA/SAC project (Somerville *et al*., 1997). In addition to the ground motions, equivalent point loads converted from the gravity loads were also applied to the beam elements to include second order effect (P-Delta effect).

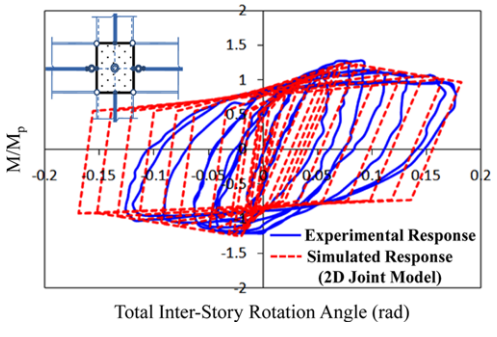

Fig. 6. Comparison of the Simulated Moment-rotation Angle Curve and the Experimental Response (Schneider and Alostaz, 1998)

6. Analyses for Composite Sections

Five points, which are anchored to P-M interaction diagrams for all composite columns presented in this study, are summarized in Table 6. They were computed in accordance with the formulas given to Tables 1 and 2.

The comparisons of analytical results obtained from numerical experiments with the formulas provide the significant opportunity to investigate the behavior of high strength CFT beam-columns and prove the validity of applied theory. For the section analyses, composite CFT cross sections are simply modeled as numerical fiber sections shown in Fig. 7(a). Numerical CFT beam-column specimens made up of flexible zero-length elements with discrete fiber sub-regions (e.g. quadrilateral, circular, and triangular shapes) were generated by the OpenSEES program. The numerical test results obtained by fiber section analyses can provide sufficient findings to estimate the capacity of composite CFT sections.

The fiber sections contained the nonlinear stress-strain response properties as illustrated in Fig 4. Numerical analyses require the hysteretic stress-strain behavior. The cyclic stress-strain behavior

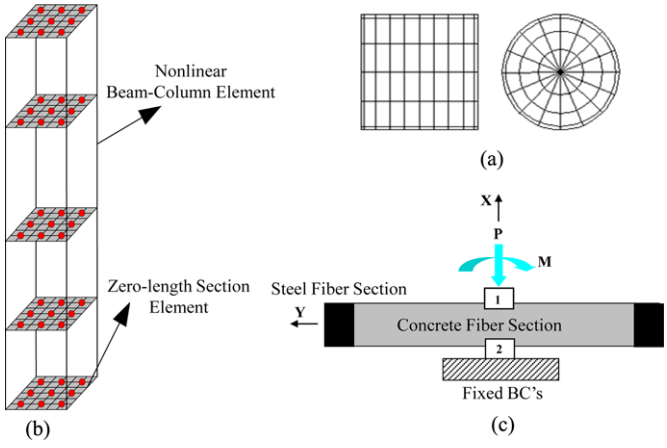

Fig. 7. Numerical Models and Test Setup for the Fiber Analyses

Table 6. All Calculation Results for Five Points in Nominal P-M Interaction Diagrams

Point	HSS 406X406X12		HSS 406X406X16		HSS 356X356X16		HSS 254X254X10		HSS 457X12		HSS 508X12		HSS 286X12	
	P*	M**	P	M	P	M	P	M	P	M	P	M	P	M
(A)	9739	0	11147	0	9294	0	4245	0	8966	0	10507	0	4546	0
(E)	5093	869	5402	1062	4306	801	2086	250	7350	388	8733	474	3491	155
(C)	3400	1041	3288	1260	2457	945	1293	297	3834	773	4789	960	1394	290
(D)	1700	1099	1644	1307	1228	972	647	309	1917	902	2395	1147	697	313
(B)	0	1041	0	1260	0	945	0	297	0	773	0	960	0	290

* Unit is kN. ** Unit is kN-m.

of steel fibers included the effects of isotropic strain hardening, Bauschinger behavior, and biaxial stress, while that of concrete fibers included the effects of stress degradation, crack opening, and crack closing.

As shown in Fig. 7(b), the fiber section-based zero-length elements were added to the nonlinear beam-column element at the integration points. Both member forces and deformations were collected using the element recorder tool at each integration point. These integration points can be converted into simple zero-length section element to represent the force-deformation relationship for the cross section of the beam-column ($P-\varepsilon$ and $M-\phi$).

Numerical test setup for the section analysis with a zero-length section element is shown in Fig. 7(c). Zero-length section elements connect two points at the same position. The test section element was subjected to the various levels for the axial force with the bottom node fixed, and then the moment curvature response was applied to measure the moment capacity at each fixed axial load level. Therefore, interactive bending moments corresponding to each axial force level were obtained on the plastic moment curvature (ϕ_P) at the curves shown in Fig. 8(a). For instance, the interactive bending moment corresponding to the balance axial force level, which is P_D=1644 kN, results in M_D=1290 kN-m on the plastic moment curvature. This plastic moment curvature can be calculated by dividing the yield strain of the steel tube into the half width of inside concrete (e.g. $\phi_P = 2\varepsilon_y/h_2$).

On the basis of the numerical test results which were performed on the fiber section element, P-M interaction diagram for a composite section can be developed as detecting the plastic-flexural strength at each axial load level. The comparison of P-M interaction strength is shown in Fig. 8(b). Both compared P-M interaction curves show good agreement, meaning that numerical test results are reasonable to evaluate the capacity of the composite CFT column section accurately.

The axial strength calculated needs to be adjusted to account for the length effect through Table 3. The adjustment depends on the ratio of P_o/P_e corresponding to the column slenderness ratio a^2 also defined in Table 3. The frame models were designed with the effective column length of either 3.96 m or 5.49 m for the story height. The maximum axial strength for composite CFT columns, including the stability reduction, can be determined in accordance with the compressive axial strength curve which was

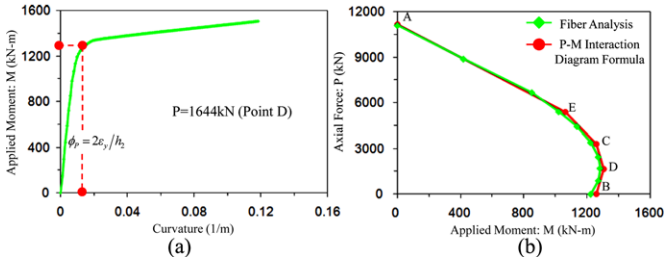

Fig. 8. Formation of P-M Interaction Diagrams (RCFT 405×406×16 Column): (a) Moment-Curvature Test under Fixed Axial Loading, (b) P-M Interaction Diagram

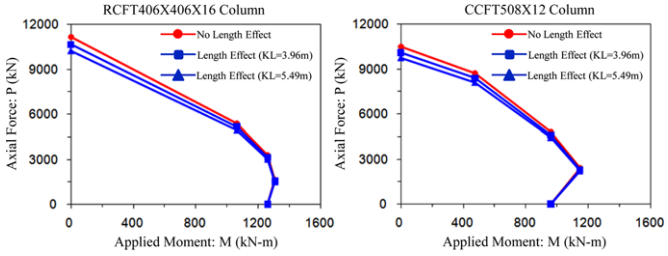

Fig. 9. P-M Interaction Diagrams Including Length Effect

obtained on the effective column length (e.g. P_{cr}=10670 kN for the column length of 3.96 m). The stability reduction should be included in other axial strength points. The stability reduction factor is defined as the compressive strength ratio of P_{cr} to P_A. The adjusted axial strength was obtained by the product of the original axial strength capacity to this reduction factor. Fig. 9 shows P-M interaction diagrams for some selected CFT columns including the length effect. This length effect can be ignored at the dominant flexural strength points such as Points (D) and (B).

7. Performance Evaluation

The principal objective in the seismic design of moment frames is to provide sufficient strength and deformation capacity on a member-by-member basis so that collapse does not occur under maximum credible ground motion. Especially, the exceedance of any ultimate limit state in the columns indicates the most severe type of damage for the building as it can lead to complete collapse. Therefore, a careful investigation of the structural damage for the composite columns is emphasized in this section. In general, the more popular available design-oriented programs do not provide the correct design checks for the beam-columns and composite sections in particular. In addition, the design checks would not provide any information on actual performance. Most of all, there were no existing investigations on either seismic performance or damage evaluation for composite-moment frames. This section focuses on the seismic performance and the damage evaluation for composite CFT columns because of these reasons.

Only data at some key location can be examined in detail because all frame models are symmetric in plan and subjected to uniform gravity loads along all bays and stories. The values for damage evaluation show a similar distribution along the representative lines of the composite columns. Identifications for nodes and members to be used in this discussion are given in Fig. 2(c). The first number in the column ID indicates the position of the column line, while the last number indicates the story level (e.g. 1C1B). Each story level has two measurement points located on the bottom (B) and top (T) of the CFT column.

There are two major steps in performing the damage evaluation, one associated with determining the capacity and the other with assessing the demand as mentioned above. In the first step, the cross-sectional capacity of hinging regions must be carefully determined. The ultimate capacities for rectangular/circular CFT beam-columns were estimated by using the P-M interaction

diagrams as shown in Fig. 9. In the second step, the demand at the critical sections must be established from the detailed numerical analyses of entire structures. Any damage in CFT columns can be detected by the observation that the local member forces obtained from nonlinear frame analyses exceed the strength limit defined by the P-M interaction diagram.

The member forces anchored to the domain of the P-M interaction diagram during nonlinear dynamic analyses are investigated as shown in Fig. 10. The 9SRCFT frame model subjected to LA28 ground motion was selected for the seismic evaluation. The peak member forces measured at the base of the column (e.g. P=2195 kN and M=1512 kN-m at 5.02 second; 2C1B) exceeded the strength limit. The strength limit results in the conservative estimation for composite column bases at the peak demand because the base steel materials applied to the numerical frame models contain the strain hardening effect up to the state of the ultimate stress. On the other hand, the peak member force at the 2C2T point was within the strength limit (e.g. P = 1865 kN and M = -1095 kN-m at 4.66 second).

The peak member forces for the 9SRCFT frame model under 40 ground motions are plotted on the P-M interaction diagram as shown in Fig. 11. Most of peak member forces at the column bases were distributed outside the strength limit. The peak bending moments were distributed over the wide range on the P-M interaction diagram in comparison with the peak axial forces. It was attributed to the discrepancy between applied lateral forces due to the different ground motions. The bending moments transmitted from lateral loads contribute predominately to creating plastic hinges and deformations at the column members. Most of the peak member forces measured at the 2C2T point were placed on the safe region. As expected, the level of their axial forces was slightly lower than that of axial forces at the column base.

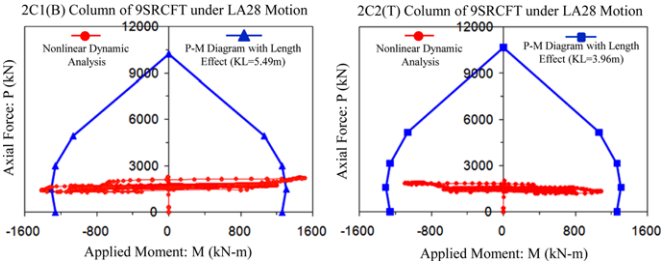

Fig. 10. Investigation of Axial Force and Moment Responses during Nonlinear Dynamic Analyses

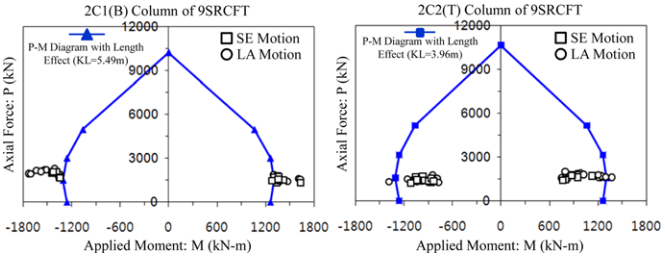

Fig. 11. Investigation of Peak Axial Force and Moment Responses during Nonlinear Dynamic Analyses

The structural damage was estimated in this study through the comparisons of the Plastic Strength Ratios (PSRs). Thus, the value of the PSR was determined by the position of the required axial force (P) and bending moment (M) on the domain of a P-M interaction diagram. The PSR method on the basis of the polygonal interaction envelope is illustrated in Table 7. The number of equations and checks needed increases as the number of points used to define the interaction envelope increases. The complete set of equations for the case of five points was used for a possible polygonal approach when the column was subjected to compression. Four regions were indentified insofar as the axial force was concerned. If the required axial strength is lower than the axial strength capacity at the balance point (PP_D), the behavior of CFT columns is controlled by yielding in tension due to the bending moments. The behavior in this region is very ductile. Otherwise ($P>P_D$), the behavior of CFT columns will be gradually dominated by the axial load. Once the plastic failure begins at the composite column, the value of the PSR exceeds the value of 1.0. This evaluation approach is very convenient to check the damage of the entire frame structure subjected to the seismic loads.

240 simulations were performed for nonlinear dynamic analyses using 40 SAC ground motions. To investigate the vast extent of analytical results effectively, the peak responses of frame models subjected to each ground motion should be examined using the statistical approach. The graphs of the scatter data for peak PSRs distributed over the story height are provide in Fig. 12. The graphs also show the statistically characteristic values such as median and 84 percentile PSRs as described in FEMA 355C together with individual peak data points. The peak PSR values for two frame models (3SRCFT and 9SRCFT) under 40 ground motions were computed at the time when the maximum base shear force occurred. The larger PSRs were distributed to LA ground motions having larger PGAs as compared with SE ground motions. The dashed lines indicate the limit of 1.0 PSR value. Severe plastic damage occurs at the lower story of the building where the larger

Table 7. Full Plastic Strength Ratio Approach Based on Polygonal Interaction Envelope

FULL PLASTIC STRENGTH RATIO BASED ON POLYGONAL INTERACTION ENVELOPE	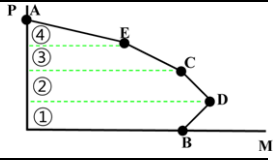

Decision	Defining Equations
① $0 < P \le P_D$ $\overline{BD}$ Line	$PSR = \frac{M}{M_B} + \left(1 + \frac{M_D}{M_B}\right)\frac{P}{P_D} \le 1.0$
② $P_D < P \le P_C$ $\overline{DC}$ Line	$PSR = \frac{P_D - P_C}{M_C P_D - M_D P_C} M + \frac{M_C - M_D}{M_C P_D - M_D P_C} P \le 1.0$
③ $P_C < P \le P_E$ $\overline{CE}$ Line	$PSR = \frac{P_C - P_E}{M_E P_C - M_C P_E} M + \frac{M_E - M_C}{M_E P_C - M_C P_E} P \le 1.0$
④ $P_E < P \le P_A$ $\overline{EA}$ Line	$PSR = \left(\frac{P_E}{P_A} - 1\right)\frac{M}{M_E} + \frac{P}{P_A} < 1.0$

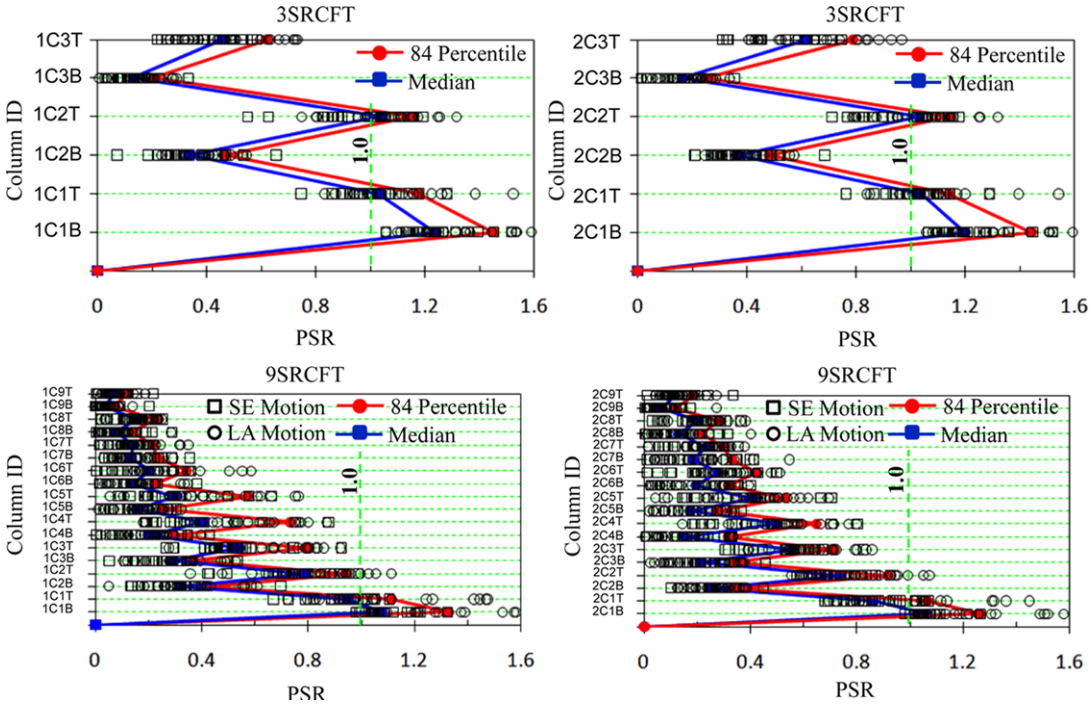

Fig. 12. Statistical Investigation of the Peak PSRs under 40 Original Ground Motions

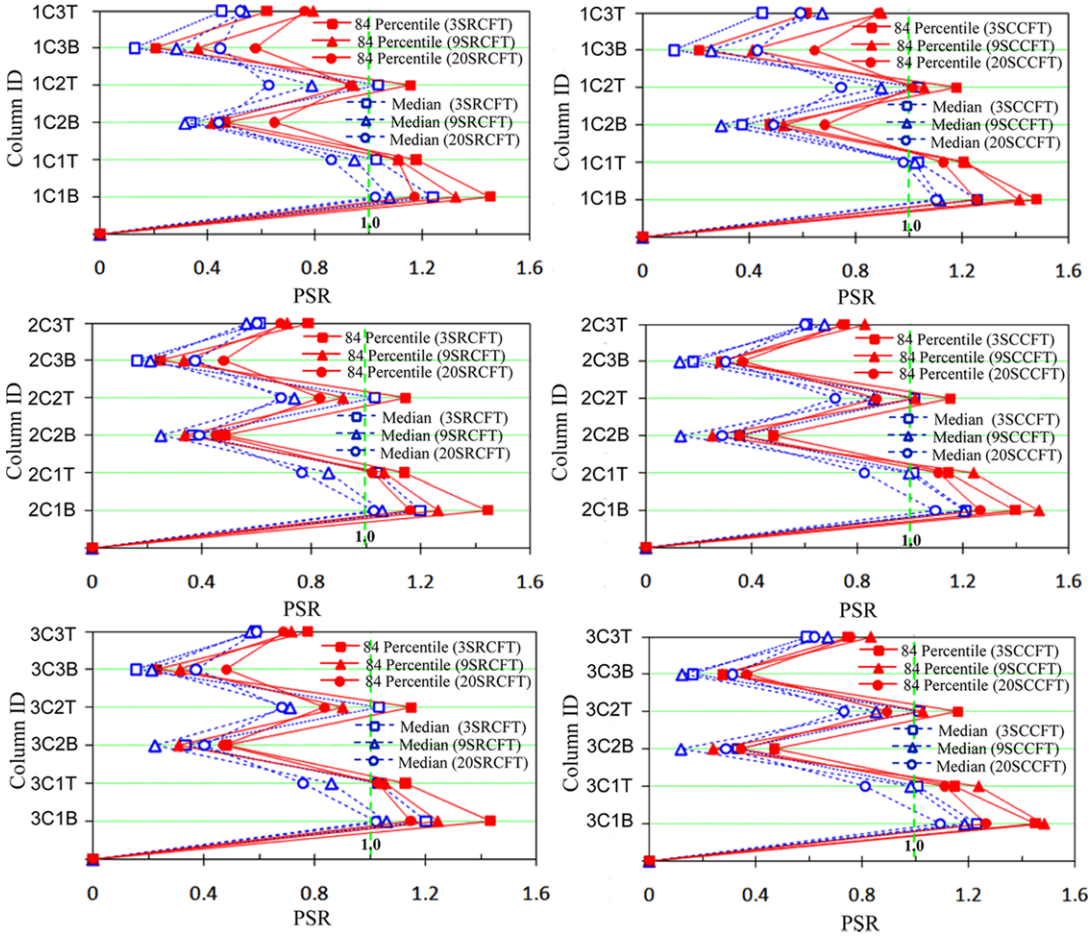

Fig. 13. Statistical Investigation of the Peak PSRs for All Frame Models under 40 Original Ground Motions

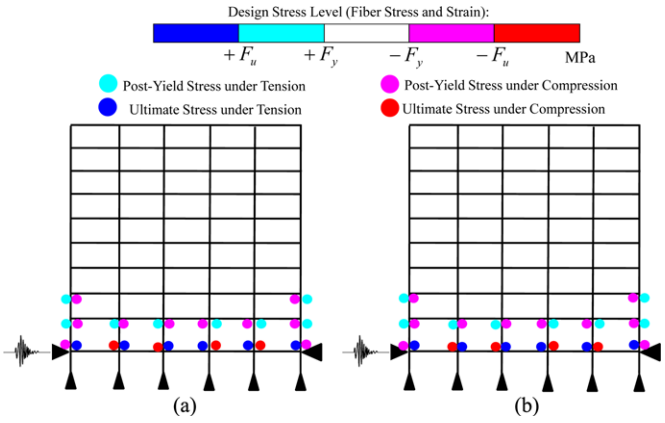

Fig. 14. Investigation of the Stress Hinges During Nonlinear Dynamic Analyses

PSRs are concentrated. Especially, the column bases failed as their PSR exceeds the average value of approximately 1.20. The values less than 1.0 were distributed over more than third story level. This indicates that the possibility of failure is relatively lower. To examine the structural damage occurring at the lower story level with more details, the statistical values of peak PSRs for all frame models computed within the third story level are summarized in Fig. 13. The frame models with the same column shapes are compared with these statistical values. 3RCFT frame model experienced the relatively higher statistical value of PSRs as compared with 9SRCFT and 20SRCFT frame model. All statistical values at the column bases exceeded the 1.0 PSR limit. Besides, 84 percentile PSRs for all frame models also were above this limit at the top of first-story columns.

The stress hinges during nonlinear dynamic analyses are shown in Fig. 14. The stress levels such as yield and ultimate stress were determined from the nominal design strength values of base steel materials in the composite columns (e.g. FE350 or FE310 carbon steel). The state of the hinge (i.e. the yield stress hinge or the ultimate failure hinge) was determined from the fiber stresses which were measured at the integration points of the nonlinear beam-column elements. The hinges were computed at the time of the highest demand on the 9-story frame models. The maximum demand, which implies severe damage and plastic deformation, also concentrated on the column bases. The location of stress hinges was symmetric with respect to the center of the moment frames. Overall, the distribution of stress hinges coincided with the position where the statistical values of PSRs exceed the 1.0 limit. As a result, the adequacy of the damage evaluation through the PSRs can be verified by examining the sequence of stress hinge formation.

8. Conclusions

The 2005 AISC specification has been used to estimate composite beam-column strength, accounting for stability effects on column members subjected to axial compression plus flexural bending moment. P-M interaction curves obtained by fiber analysis results show good agreement with P-M interaction diagrams calculated from P-M interaction formulas. It indicates that full plastic capacities applied to this design specification are quite reasonable to predict the interaction strength for composite beam-columns. The P-M interaction diagrams based on the beneficial effect of composite sections were applied to the damage evaluation for the entire composite-moment frame. The SAC post-Northridge building models with C-SMF systems were designed for nonlinear frame analyses. The statistical distribution of peak PSRs was obtained from the nonlinear dynamic analyses. The peak PSRs showed the largest values at the bases of composite columns. They decrease as one moves up the frame structure. The sequence of stress hinge formation conformed to the distribution of statistical PSR values which exceed the 1.0 limit for safety. Finally, it is concluded that the PSR proposed in this study was the useful index to determine whether the composite columns at the frame structure reach the failure state.

Notations

A_c: Cross section area of a concrete core
A_s: Cross section area of a steel tube
E_c: Elastic modulus of concrete ($E_c = 4700\sqrt{f'_{cc}}$ MPa)
E_s: Elastic modulus of steel
EI_{eff}: Effective elastic stiffness of a composite section
I_c: Moment inertia of a concrete core
I_s: Moment inertia of a steel tube
KL: Effective height of the composite column
F_y: Yield stress of steel (e.g. F_y=350 MPa for FE350 carbon steel)
F_u: Ultimate stress of steel (e.g. F_u=590 MPa for FE350 carbon steel)
M: Applied moment
M_A=...=M_E: Available flexural strength (Capital subscript indicates the observed point)
P: Applied axial force
P_A=...=P_E: Available axial strength (Capital subscript indicates the observed point)
P_{cr}: Nominal compressive strength for the composite column with the stability effect
P_e: Euler compressive column strength
P_o: Nominal compressive strength for the composite column without the stability effect
P_u: Ultimate compressive strength for the composite column
$Z_{sB} - Z_{sE}$: Plastic section modulus of steel shape at Points (B) and (E)
Z_{cB}=Z_{cE}: Plastic section modulus of concrete shape at Points (B) and (E)
b: Width of the composite section
d: Depth or diameter of the composite section
d_b: Depth of the steel beam
d_c: Depth of the composite column
f_c: Uni-axial compressive strength for concrete

f'_c: Crushing strength of unconfined concrete
f'_{cc}: Crushing strength of confined concrete
f_{ct}: Tensile strength of concrete
f_l: Lateral confining pressure
f_t: Uni-axial tensile strength for concrete
h: Height of the concrete core (e.g. $h_2 = d - 2t_f$)
h_n=h_E: Equivalent height of the composite section between center and PNA
k_3: Material degradation parameter
r_m: Effective radius of the CFT section
t: Thickness of the steel tube
t_w: Thickness of the web of the steel tube
t_f: Thickness of the flange of the steel tube
V: Shear force acting on the panel zone
α: Slenderness ratio of the composite column
ε_c: Uni-axial compressive strain for concrete
ε'_c: Uni-axial compressive strain of unconfined concrete corresponding to f'_c
ε'_{cc}: Uni-axial compressive strain of confined concrete corresponding to f'_{cc}
ε_{ct}: Tensile strain of concrete corresponding to f_{ct}
ε_t: Uni-axial tensile strain for concrete
ϕ: Yield strain of the steel tube
ϕ: Moment curvature of the composite section
ϕ_p: Plastic moment curvature of the composite section
γ: Deformation of the panel zone due to shear force
θ: Arc angle

Acknowledgements

This research was partially supported by WCU (World Class University) program through the NRF (National Research Foundation) of Korea funded by the Ministry of Education, Science and Technology (Grant No. R32-2008-000-20042-0). The corresponding author (J.W. Hu) would like to thank not only the National Science Foundation (NSF) for six years of financial support (US Grant No. 0324542) as a research assistantship and a post-doctorate fellowship at Georgia Tech, but also the Korean Science and Engineering Foundation (KOSEF) for two years of financial support (Grant No. M06-2003-000-10009-0) as a government graduate scholarship student.

References

Altoontash, A. (2004). *Simulations and damage models for performance assessment of reinforced concrete beam-column joints*, Ph.D. Dissertation. Stanford University, CA., USA.

American Institute of Steel Construction (AISC) (2001). *Manual of steel construction: Load and Resistance Factor Design (LRFD)*. 3rd edition. Chicago, IL., USA.

American Institute of Steel Construction (AISC) (2005). *Seismic provisions for structural steel buildings (ANSI/AISC 341-05)*. Chicago, IL., USA.

American Institute of Steel Construction (AISC) (2005). *Specification for structural steel buildings (ANSI/AISC 360-05)*. Chicago, IL., USA.

American Society of Civil Engineers (ASCE) (2005). *Minimum Design loads for buildings and other structures (ASCE/SEI No. 7-05)*. Reston, VA., USA.

Asgarian, B., Sadrinezhad, A., and Alanjari, P. (2010). "Seismic performance evaluation of steel moment resisting frames through incremental dynamic analysis." *Journal of Constructional Steel Research,* Vol. 66, pp. 178-190.

Azizinamini, A. and Schneider, S.P. (2004). "Moment connections to concrete-filled steel tubes." *Journal of Structural Engineering*, ASCE, Vol. 130, No. 2, pp. 213-222.

Calambos, T. V. (2000). "Recent research and design developments in steel and composite steel-concrete structures in USA." *Journal of Constructional Steel Research,* Vol. 55, No. 1-3, pp. 289-303.

Chin, W. I., Kang, J. Y., Choi, E. S., and Lee, J. W. (2009). "A study on the flexual behavior of concrete filled steel tube girder on parametrically varied filling and composition." The KSCE Journal of Civil Engineering, Vol. 29, No. 2, pp. 109-118.

FEMA-355C (2000). *State of the art report on systems performance of steel moment frames subjected to earthquake ground shaking*. FEMA 355C/September 2000. Washington (DC): Building Seismic Safety Council.

Grecea, D., Dinu, F., and Dubina, D. (2004). "Performance criteria for MF steel frames in seismic zones." *Journal of Constructional Steel Research,* Vol. 60, pp. 739-749.

Hu, J. W. and Leon, R. T. (2010) "Analyses and evaluations for composite-moment frames with SMA PR-CFT columns." *Nonlinear Dynamics* (DOI 10.1007/s11071-010-9903-3).

Hu, J. W., Choi, E., and Leon, R. T. (2011). "Design, analysis, and application of innovative composite PR connections between steel beams and CFT columns." *Smart Materials and Structures*, Vol. 20, No.2 (doi:10.1088/0964-1726/20/2/025019).

Hu, J. W., Kang, Y. G., Choi, D. H., and Park, T. (2010). "Seismic design and behavior of composite-moment frames with steel beam-to-concrete filled tube column connections." *International Journal of Steel Structures,* KSSC, Vol. 10, No. 2, pp. 177-191.

Hu, T., Huang, C. S., and Chen, Z. L. (2005). "Finite element analysis of CFT columns subjected to an axial compressive force and bending moment in combination." *Journal of Constructional Steel Research*, Vol. 61, No. 12, pp. 1692-1712.

Kim, Y. J., Shin, K. J., and Kim, W. J. (2008). "Effect of stiffener details on behavior of CFT column-to-beam connection." *International Journal of Steel Structures,* KSSC, Vol. 8, No. 2, pp. 119-133.

Leon, R. T. (1997). *Seismic performance of bolted and riveted connections. Background reports: Metallugy, fracture mechanics, welding, moment connections, and frame system behavior.* FEMA publication No.288. Washington (DC): Federal Emergency Management Association (FEMA).

Mazzoni, S., Mckenna, F, and Fenves, G. L. (2006). *OpenSEES command language manual v. 1.7.3.* Department of Civil Environmental Engineering. University of California, Berkley. CA., USA.

Nishiyama, I., Fujimoto, T., Fukumoto, T., and Yoshioka, K. (2004). "Inelastic force-deformation response of joint shear panels in beam-column moment connections to concrete-filled tubes." *Journal of Structural Engineering*, ASCE, Vol. 130, No. 2, pp. 244-252.

Ricles, J. M., Peng, S. W., and Lu, L.W. (2004). "Seismic behavior of composite concrete filled steel tube column-wide flange beam moment connections." *Journal of Structural Engineering*, ASCE, Vol. 130, No. 2, pp. 223-232.

Roeder, C. W. (1998). "Overview of composite systems for seismic design in the United State." *Engineering Structures,* Vol. 20, No. 4-

6, pp. 355-363.

Schneider, S. P. and Alostaz, Y. M. (1998). "Experimental behavior of connections to concrete-filled steel tubes." *Journal of Constructional Steel Research,* Vol. 45, No. 3, pp. 321-352.

Somerville, P. G., Smith, N., Punyamurthula, S., and Sun, J. (1997). *Development of ground motion time histories for phase 2 of the FEMA/SAC steel project*. SAC background document, No. SAC/BD 97/04.

Tsai, K. C., Hsiao, P. C., Wang, K. J., Weng, Y. T., Lin, M. L., Lin, K. C., Chen, C. H., Lai, J. W., and Lin, S. L. (2008). "Pseudo-dynamic tests of a full-scale CFT/BRB frame-Part I: Specimen design, experiment and analysis." *Earthquake Engineering and Structural Dynamics,* Vol. 37, pp. 1081-1098.

Wu, L. Y., Chung, L. L., Tsai, S. F., Lu, C. F., and Huang, G. L. (2005). "Seismic behavior of bolted beam to column connections for concrete filled steel tube." *Journal of Constructional Steel Research*, Vol. 61, pp. 1387-1410.

Wu, L. Y., Chung, L. L., Tsai, S. F., Lu, C. F., and Huang, G. L. (2007). "Seismic behavior of bidirectional bolted connections for CFT columns and H-beams." *Engineering Structures*, Vol. 29, No. 3, pp. 395-407.